Design, fabrication, and characterization of high-efficiency extreme ultraviolet diffusers

Patrick P. Naulleau, J. Alexander Liddle, Farhad Salmassi, Erik H. Anderson,

and Eric M. Gullikson

Center for X-Ray Optics, Lawrence Berkeley National Laboratory
1 Cyclotron Rd., Berkeley, CA 94720

As the development of extreme ultraviolet (EUV) lithography progresses, interest grows in the extension of traditional optical components to the EUV regime. The strong absorption of EUV by most materials and its extremely short wavelength, however, makes it very difficult to implement many components that are commonplace in the longer wavelength regimes. One such example is the diffuser often implemented with ordinary ground glass in the visible light regime. Here we demonstrate the fabrication of reflective EUV diffusers with high efficiency within a controllable bandwidth. Using these techniques we have fabricated diffusers with efficiencies exceeding 10% within a moderate angular single-sided bandwidth of approximately 0.06 radians.

OCIS codes: 230.1980, 260.7200, 290.5880, 340.6720, 220.4000, 230.4000

Introduction

Extreme ultraviolet (EUV) lithography [1] remains the top candidate for the technology to be used for the 32-nm generation of nano-electronics expected to enter volume production in 2009. As development of this technology progresses, the problem of extending the use of a variety of traditional optical components to the EUV regime becomes increasingly important. The strong absorption of EUV by most materials and its extremely short wavelength, however, makes it very difficult to implement many components that are commonplace in the longer wavelength regimes. One such example is the diffuser often implemented with ordinary ground glass in the visible light regime. Here we demonstrate the fabrication of reflective EUV diffusers with high efficiency within a controllable bandwidth. Using these techniques we have fabricated diffusers with efficiencies exceeding 10% within a moderate angular single-sided bandwidth of approximately 0.06 radians.

Diffusers play an important role in optics both from the standpoint of illumination uniformity control (spatial and angular) as well as coherence control [2,3]. When used for coherence control, the diffuser serves as a random phase modulator with temporal modulation being achieved by translating the diffuser within the illuminating beam. When such a system is used, for example, as the effective source in a Köhler illuminator (the source is in the back focal plane of the condenser lens), the illumination coherence can be controlled by setting the size and/or shape of the illumination spot on the ground glass. Diffuser-based coherence reduction has been proposed at EUV [4], to address the problem of performing lithography using highly coherent synchrotron sources [5,6], however, fabrication difficulties have rendered the method impractical in the past.

Transmission EUV diffusers

A direct analog of ground glass as used at visible wavelengths would be a random phase transmission screen at EUV. Unlike at visible wavelengths, however, no pure phase shifting materials exist in the EUV wavelength regime. There are, nevertheless various candidate materials that have attractive absorption to phase-shifting ratio properties. [7] One of the best available materials for phase shifting at EUV wavelengths is Molybdenum (Mo). At a wavelength of 13.4 nm, Mo has a Delta (the decrement from unity of the real part of the complex index of refraction) of 7.73×10^{-2} and a Beta (the imaginary part of the index of refraction) of 6.23×10^{-3}. From these values, we find the 1/e attenuation length of Mo to be 171 nm and the π-phase-shift length to be 86.5 nm. For a π-phase-shift thickness the transmission intensity at a wavelength of 13.4 nm is approximately 60%. As described below, this residual absorption severely limits the achievable efficiency from transmission EUV diffusers.

In the illustrative example that follows, we consider a statistically Gaussian diffuser [8] with a target diffraction numerical aperture (NA) of approximately 0.02. When considering ideal phase diffusers, the target diffraction bandwidth can be equally-well achieved by varying either the minimum feature size on the diffuser and/or the modulation-depth of the diffuser. For an EUV diffuser, however, the residual absorption leads to a significant loss in efficiency as the modulation depth is increased, thus in practice it is preferable to use spatial feature size control as the primary mechanism to achieve scatter bandwidth control. The lower limit on this modulation depth is set by the specular suppression levels required of the diffuser for its particular application.

The trade-off between modulation depth, efficiency, and specular suppression capabilities is illustrated in Table 1. The tabulated properties are determined from time-averaged far-field diffraction calculations assuming the diffuser to be moving relative to the illumination. The time

averaging, which serves to suppress the speckle, is simulated by calculating the intensity diffraction patterns for approximately 1000 independent realizations of the diffuser and averaging the results. The total power efficiency is calculated ignoring substrate effects and assuming the minimum Mo thickness to be zero. In practice, the diffuser must be patterned onto a membrane that will further attenuate the light, further diminishing the throughput. If, for example, the diffuser is patterned onto a 100-nm thick Si_3N_4 membrane, the actual efficiency will be ~43% of the numbers shown in Table 1. Moreover, achieving the proper height statistics, in practice, would likely no be possible without leaving some finite minimum thickness of Mo, further reducing the throughput.

The column referred to as efficacy in Table 1 is defined as the low-angle scatter to specular transmission ratio (Fig. 1). The modulation-depth is defined as the standard deviation of the thickness profile in π-phase-shift lengths. For example, a Mo Gaussian diffuser with a modulation-depth of 1 has a thickness standard deviation of 86.5 nm.

The modeling results show that a modulation depth of greater than 1.2 is required in order to achieve an efficacy greater than 0.96 for the approximately 0.02 NA bandwidth Molybdenum diffusers considered here. Exceeding this modulation depth causes the efficiency to quickly drop below 10%, thus complete suppression of the specular term (efficacy = 1) is likely impractical. Requiring an efficacy of unity, however, may be overly restrictive: when used for coherence control in an imaging system, the more relevant property to consider is the ratio of the, partially-coherent to coherent image strength. The specular component from the diffuser can be viewed as overlaying the desired partially-coherent image with a coherent image. The ratio of interest is, thus, the total energy contributing to the imaging over the specular energy contributing to the imaging. For the first entry in Table 1, where the efficacy is a low 0.52, we see this ratio to be

7,769 to 1 assuming that scattered light from the diffuser up to an NA of 0.025 contributes to the image (the acceptance NA of a 4×-reduction 0.1-NA system). The desired incoherent image is more than 7,000 times stronger than the coherent overlay. This tremendous gain compared to the efficacy definition is a result of the new measure taking into consideration the two-dimensional nature of the diffuser.

The claim that the incoherent image is more than 7,000 times as strong as the coherent overlay assumes the coherent and incoherent object-plane illumination areas to be equal in size. Achieving this limiting case requires the diffuser to be very close to, or re-imaged, to the object plane (*Critical Illumination*). If the diffuser lies in a Fourier transform plane relative to the object plane (*Khöler Illumination*) the coherent illumination will be concentrated [9]. In this case the coherent overlay will be more noticeable, however, it will also be limited in area.

Next we determine of the efficiency of a representative transmission diffuser. We take the example of a Gaussian diffuser with a half maximum scatter angle of 0.025 radians and a collection angle matched to the half-maximum scatter angle. We place a source print-through contrast limit of 1% on the device and assume the source NA to be 0.006. This moderate specular-suppression requirement enables the use of a modulation depth of 1 yielding a 6σ surface modulation of 519 nm. Finally we assume the diffuser to be fabricated onto a 100-nm thick Silicon Nitride membrane and assume a residual bulk Mo thickness of 50 nm (approximately 10% of the modulated Mo thickness). Under these assumptions (Table 2), we predict an efficiency of approximately 1.7% within the collection angle.

Reflection EUV diffusers

The low efficiency of the transmission EUV diffuser described above would likely render it impractical in many applications. Moreover, fabrication of such a device onto a silicon nitride

membrane is expected to be quite challenging. An alternative approach is to consider a reflection instead of a transmission diffuser. One way to fabricate a reflection EUV diffuser is to first fabricate an appropriately rough substrate and then to overcoat the substrate with a reflective EUV multilayer. To the extent that the multilayer growth is conformal to the surface, the fabricated roughness will be transferred to the multilayer. In this case, phase modulation is achieved through geometric path-length differences upon reflection as opposed to optical path-length differences achieved by propagating through materials with indices of refraction substantially different than that of vacuum.

Deterministic fabrication of such reflection EUV diffusers can be achieved using a recently demonstrated electron-beam lithography technique originally developed for the fabrication of high efficiency near-normal incidence blazed phase gratings operating in the EUV regime [10-12]. In this technique, fabrication of the desired diffuser surface is achieved directly in resist through a gray-scale electron-beam exposure process. With high resolution and low intrinsic roughness, hydrogen silsesquioxane (HSQ) [13], a spin on glass made by Dow Corning, has proven ideal for the fabrication of diffractive EUV phase structures. Another benefit of this material is that it is extremely stable after development, serving as a good permanent base for the requisite multilayer overcoat [10].

A significant benefit of the reflection diffuser is that the required topography is significantly smaller than for a transmission diffuser. This is a result of the geometric phase modulation mechanism. Moreover, reflection devices provide nearly pure phase modulation allowing smaller modulation depth to be used while still achieving high extinction of the specular component. Although the reflection diffuser geometric phase modulation mechanism allows the topography to be significantly reduced compared to a transmission diffuser, strictly

speaking a true Geometric diffuser [8] could still require arbitrarily large topography because there remains a finite probability of any height. This would be a significant problem for the gray-scale direct patterning method. Restricting the allowable topography to a height range of +/-3 σ, where σ is the standard deviation of the desired diffuser, can eliminate this potential problem while having negligible effect on the diffuser performance. Targeting a relatively safe modulation depth of 1.1, a wavelength of 13.4 nm, and an angle of incidence of 5°, we find the required diffuser σ to be 3.70 nm and the total diffuser height modulation to be 22.2 nm. Although significantly smaller then 519-nm modulation required of the transmission diffuser, the 22.2 nm value is still approximately 4 times larger than the modulation previously implemented for EUV gratings.

It is important to point out that the topography requirements stated above apply to the coated diffuser, not simply the patterned HSQ. Multilayer-induced planarization thus requires the topography in HSQ to be even larger. Based on experimental results with magnetron-sputtered multilayers, we have found the actual required HSQ topography to approach 30 nm when fabricating a 100-nm correlation length diffuser. It is also evident that as the desired correlation length is decreased or the multilayer planarization effects are increased, the required HSQ topography will further increase.

Reflection diffusers fabrication

The first step in the diffuser fabrication process is to define the exposure data set. To facilitate this process we implement cell diffusers where the diffuser is defined as a regular checkerboard pattern with the height of each square being assigned a random height from a Gaussian distribution (Fig. 2). The scatter angle range of the resulting diffuser will be fully defined by the cell size. This can be seen by representing the cell diffuser as a two-dimensional comb function

comprised of randomly phased delta functions convolved with a square two-dimensional rect function. Under this representation, diffraction from the random phase comb will create a random speckle pattern that is multiplied by the diffraction from the rect function providing the envelope. Alternatively, we can simply take the diffuser correlation length to be equal to the cell size. For the diffuser described here we target a correlation length of 100 nm providing a half-maximum intensity half angle of 0.059 radians.

The next step in the fabrication process is to determine the correspondence between exposure dose and remaining resist thickness or height. It is not sufficient to simply use conventional contrast curves as these are typically derived from large open field exposures and do not account for proximity effects in the exposure itself or the resist, which can be significant over the length scales of interest here (100-nm and smaller). This problem is illustrated in Fig 3 where atomic force microscope (AFM) images of a single 3-μm wedge and alternating polarity 100-nm wide wedges are shown. In each case the target wedge height was approximately 35 nm. For the wide feature, it is evident that the conventionally measured resist contrast curve served as a good calibration whereas in the case of the narrow features the achieved modulation (Fig. 4) is approximately 10-nm (29%) smaller than desired. The observed nonlinearity of the modulation is likely the result of the intrinsic roughness playing an increasingly important role as the modulation is decreased.

In light of the relevance of proximity issues for gray-scale patterning at length scales relevant to EUV diffusers, we build up a process modulation curve by exposing a series of simple two-dose checkerboard patterns where the differential dose is changed at each point in the series. Figure 5 shows the prescribed exposure pattern and an AFM image of representative

exposure from the series. Based on this calibration, the desired height profile can be converted to an exposure dose profile.

Using these methods, a ~100-nm correlation length diffuser has been fabricated covering an area 0.6×1.8 mm. The diffuser was exposed into a 360-nm thick layer of HSQ resist using a high-resolution electron-beam lithography tool [14,15] operating at 100 keV. The base exposure dose was approximately 100 $\mu C/cm^2$. After exposure, the HSQ is developed in 0.26N TMAH photoresist developer, Shipley LDD26W for 120 seconds. Next the patterned HSQ surface is overcoated with a magnetron sputtered [16] EUV reflective Mo/Si multilayer. The multilayer is designed for near-normal incidence and a wavelength of 13.4 nm. The multilayer was comprised of a total of 40 bilayers with a bilayer thickness of approximately 7 nm. In the case of the 100-nm-correlation-length diffuser, magnetron coating has been found to be preferable over ion-beam deposition [17] due to the lower smoothing of the patterned roughness. Figure 6 shows an AFM image of the final diffuser along with the normalized histogram of the surface heights (approximation of the probability density function). The measured σ of the surface is approximately 3.77 nm, meeting the design requirement described above.

The fabricated diffuser was characterized at 13.4 nm and an angle of incidence of 5° using the high accuracy EUV reflectometer at the calibration and standards bend-magnet beamline 6.3.2 at the Advanced Light Source located at Lawrence Berkeley National Laboratory [18]. The measurement was performed with a spectral resolution, $\lambda/\Delta\lambda$, of approximately 1400. The diffuser was characterized by placing a detector at the re-imaging plane of the exit slit of the beamline monochromator and scanning the detector through the diffraction pattern. Although the 200-μm wide illuminating beam was significantly smaller than the patterned area, to further ensure the accuracy of the measured specular component, a tilted 200-μm aperture was directly

mounted to the diffuser. This allows the true specular component from the diffuser to be distinguished from any potential illumination spill over as the spill over is directed at a different angle.

Figure 7 shows a line scan through the center of the far-field diffraction pattern. The overlain smoothed curve is a fit to the data showing that the diffraction pattern is well approximated out to approximately 4° by a Lorentzian-squared function. No significant specular peak is observed. The measured total efficiency of the diffuser is 20.6% and the efficiency within the target 100-nm correlation length (0.059 radian collection angle) is 10.3%. The scatter intensity at the extreme target angle is approximately 42%, slightly lower than the 50% design value. This slight reduction in scatter bandwidth is due to the process-induced smoothing of the ideally sharp-edged cells. We note that assuming an efficacy of 0.96, as defined in section 2, a transmission Mo diffuser fabricated onto a 100-nm-thick silicon nitride membrane would have an ideal total efficiency of approximately 4%, 5 times lower then the demonstrated efficiency of the HSQ reflection diffuser.

Non-deterministic fabrication of reflective EUV diffusers

Although the gray-scale direct patterning method gray-scale direct patterning method has been demonstrated to yield efficient EUV diffusers, the exposure step is extremely slow. Using HSQ resist, the total exposure time for a 1-mm^2 diffuser in our system is approximately 6 hours. Admittedly, a significant portion of that time is stage and data-path limited, nevertheless considering the resist exposure time alone still yields a 50-minute write for a 1-mm^2 area. Such lengthy exposure times render the method infeasible for large area diffusers. To address this issue, we have also studied the generation of controlled roughness through sputtering. To date our best results have been achieved using magnetron-sputtered chrome.

The roughness generated using the sputtered chrome technique can, to some extent, be controlled through manipulation of the energetics and target distance parameters. A particularly appealing attribute of this method is its ability to generate nearly arbitrarily large diffusers. In our sputtering chamber 100-mm diameter parts can readily be coated producing nearly 8,000 mm^2 of diffuser area in less than one hour.

Figure 8 shows the EUV scatterometry characterization results for a diffuser fabricated using this process. The EUV-reflective multilayer properties are as described for the HSQ diffuser. In this case the scatter profile is well fit by a Gaussian distribution. As with the HSQ diffuser, no significant specular peak is observed. The measured total efficiency of the diffuser is 14.9%, whereas the efficiency within the target 100-nm correlation length (0.059 radian collection angle) is only 2.2%. As evidenced by these results, a significant drawback of this method is that it is very difficult to control correlation length of the fabricated diffuser resulting in much less control over the diffusion characteristics and often leading to a negative impact on the efficiency compared to an optimized HSQ diffuser.

Summary

A process enabling the controlled fabrication of EUV diffusers has been demonstrated. This method has been used to generate EUV diffusers obtaining greater than 20% total efficiency (within all scattered angles) and greater than 10% efficiency within the target collection angle. The grayscale direct patterning approach has been shown to yield considerably higher efficiency than sputter material diffusers, however, if large area devices are required, the sputtered material approach is likely preferable.

The authors are greatly indebted to Bruce Harteneck and Eugene Veklerov for expert programming and fabrication support, to Andrew Aquila for EUV metrology support, and to the

entire CXRO staff for enabling this research. This research was performed at Lawrence Berkeley National Laboratory, which is operated under the auspices of the Director, Office of Science, Office of Basic Energy Science, of the US Department of Energy.

References

1. R. Stulen and D. Sweeney, "Extreme ultraviolet lithography," IEEE J. Quantum Electron. **35**, 694-699 (1999).
2. M. V. R. K. Murty, "Interference between wave fronts rotated or reversed with respect to each other and its relation to spatial coherence," J. Opt. Soc. Am. **54**, 1187-1190 (1964).
3. W. Martienssen and E. Spiller, "Coherence and Fluctuations in Light Beams," Am. J. Phys. **32**, 919-926 (1964).
4. P. Naulleau, K. Goldberg, E. Anderson, P. Batson, P. Denham, S. Rekawa, and J. Bokor, "Adding static printing capabilities to the EUV phase-shifting point diffraction interferometer," Proceedings of the SPIE Vol. **4343**, 639-645 (2001).
5. D. Attwood, P. Naulleau, K. Goldberg, E. Tejnil, C. Chang, R. Beguiristain, P. Batson, J. Bokor, E. Gullikson, H. Medecki, and J. Underwood, "Tunable coherent radiation in the soft X-ray and extreme ultraviolet spectral regions," IEEE J. Quantum Electron. 35, 709-720 (1999).
6. C. Chang, P. Naulleau, E. Anderson, and D. Attwood, "Spatial coherence characterization of undulator radiation," Opt. Comm. **182**, 24-34 (2000).
7. B. L. Henke, E. M. Gullikson, and J. C. Davis. "X-ray interactions: photoabsorption, scattering, transmission, and reflection at E=50-30000 eV, Z=1-92," Atomic Data and Nuclear Data Tables, **54**, 181-342 (1993).
8. J. W. Goodman, *Statistical Optics*, John Wiley & Sons, New York, 1986, **Chap. 8**, 361-464.

9. J. W. Goodman, *Statistical Optics*, John Wiley & Sons, New York, 1986, **Chap. 7**, 286-360.
10. P. Naulleau, E. Anderson, E. Gullikson, and J. Bokor "Fabrication of high-efficiency multilayer-coated binary blazed gratings in the EUV regime," Opt. Comm. **200**, 27-34 (2001).
11. P. Naulleau, J. A. Liddle, E. H. Anderson, E. M. Gullikson, P. Mirkarimi, F. Salmassi, and E. Spiller, "Fabrication of high-efficiency multilayer-coated gratings for the EUV regime using e-beam patterned substrates," Opt. Comm. **229**, 109-116 (2003).
12. J. A. Liddle, F. Salmassi, P. Naulleau and E. Gullikson, "Nanoscale topography control for the fabrication of advanced diffractive optics," J. Vac. Sci. Technol. B **21**, 2980-2984 (2003).
13. F. van Delft, J. Weterings, A. van Langen-Suurling, H. Romijn, "Hydrogen silsesquioxane/novolak bilayer resist for high aspect ratio nanoscale electron-beam lithography," J. Vac. Sci. Technol. B **18**, 3419-3423 (2000).
14. E. H. Anderson, V. Boegli, and L. P. Muray, "Electron beam lithography digital pattern generator and electronics for generalized curvlinear structures," J. Vac. Sci. Technol. B **13**, 2529-2534 (1995).
15. E. H. Anderson, D. L. Olynick, B. Harteneck, E. Veklerov, Gregory Denbeaux, W. Chao, A. Lucero, L. Johnson, and D. Attwood, "Nanofabrication and diffractive optics for high-resolution x-ray applications," J.Vac. Sci. Technol. B **18**, 2970-2975 (2000).
16. D. Stearns, R. Rosen,and S. Vernon, "Fabrication of high-reflectance Mo-Si multilayer mirrors by planar-magnetron sputtering," J. Vac. Sci. Technol. A **9**, 2662-2669 (1991).
17. E. Spiller, S. Baker, P. Mirkarimi, V. Sperry, E. Gullikson, and D. Stearns, "High Performance Mo/Si Multilayer Coatings for EUV Lithography using Ion Beam deposition," Appl. Opt. **42**, 4049-4068, (2003).

18. E. M. Gullikson, S. Mrowka, B. Kaufmann, “Recent Developments in EUV Reflectometry at the Advanced Light Source,” Proc. SPIE Vol. 4343, 363-373 (2001).

List of Figures

1. Definition of diffuser efficacy based on time averaged diffraction calculations assuming a moving diffuser.
2. Exposure dataset definition for a deterministically fabricated Gaussian diffuser. The diffuser is defined as a grid of square cells where the height of each cell is assigned a random number from a Gaussian distribution limited to values falling within +/-3σ from the mean.
3. Demonstration of the relevance of proximity effects in small length scale direct gray-scale patterning of resist. (a) AFM image of patterned large 3-μm wedge in resist. Large features are relatively unaffected by proximity effects enabling the target 35-nm modulation to be achieved. (b) Prescription for alternating polarity 100-nm wide wedge pattern and (c) AFM image of corresponding patterned structure in resist suffering from approximately 10% loss in modulation.
4. Calculated position dependent peak-to-valley modulation from the AFM image in Fig. 3(c). Each point in the plot corresponds to a separate row in the patterned structure from Fig. 3(c). The high modulation edges in the plot correspond the top and bottom rows the structure in Fig. 3(c) and the low modulation center of plot corresponds to central row in the patterned structure.
5. Representative exposure pattern (a) and AFM image of print (b) for modulation calibration accounting for proximity effects. The exposure pattern is a checkerboard comprised of 100-nm squares at two different doses. The complete calibration is based on a series of exposures each with a different relative dose between the two levels. The process is also repeated for a series of different nominal dose values.

6. (a) AFM image of multiplayer coated HSQ diffuser and (b) normalized histogram of height distributions (approximation of the probability density function).
7. Line scan through the center of the measured far-field EUV diffraction pattern from the e-beam fabricated diffuser. No significant specular peak is observed. The measured total efficiency of the diffuser is 20.6% and the efficiency within the target 100-nm correlation length (0.059 radian collection angle) is 10.3%.
8. Line scan through the center of the measured far-field EUV diffraction pattern from the sputtered chrome diffuser. No significant specular peak is observed. The measured total efficiency of the diffuser is 14.9% and the efficiency within the target 100-nm correlation length (0.059 radian collection angle) is 2.2%.

List of Tables

1. Mo transmission diffuser properties as a function of modulation depth.

2. Mo transmission diffuser case study.

Modulation depth	Efficacy	Total power efficiency (%)
1.0	0.52	13.8
1.1	0.82	11.5
1.2	0.96	9.7
1.4	0.98	6.8
4.0	1.00	0.9

Table 1. Mo transmission diffuser properties as a function of modulation depth.

100-nm Silicon Nitride throughput	0.43
50-nm bulk Mo throughput	0.75
Modulated Mo throughput	0.12
Collected area fraction	0.45
Total efficiency	**0.017**

Table 2. Mo transmission diffuser case study.

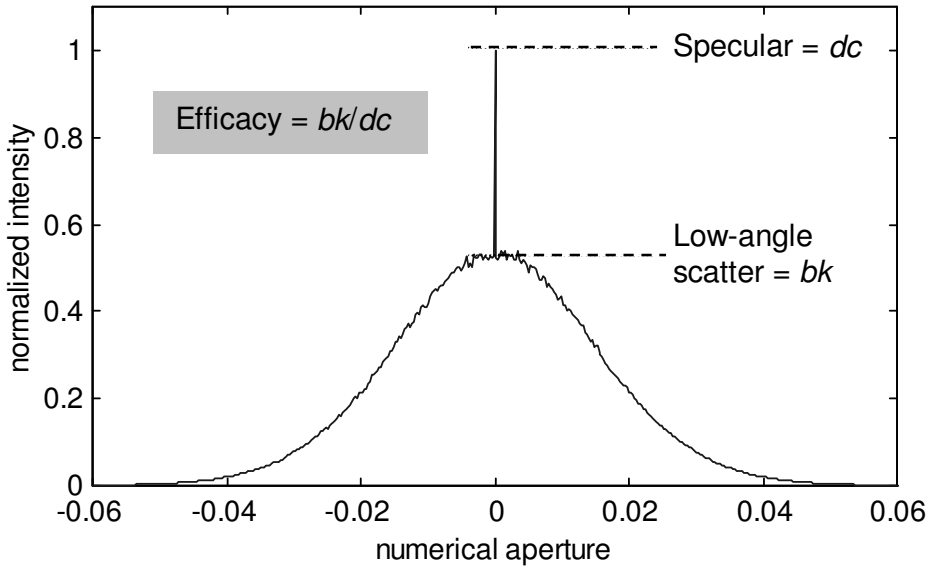

Fig. 1. Definition of diffuser efficacy based on time averaged diffraction calculations assuming a moving diffuser.

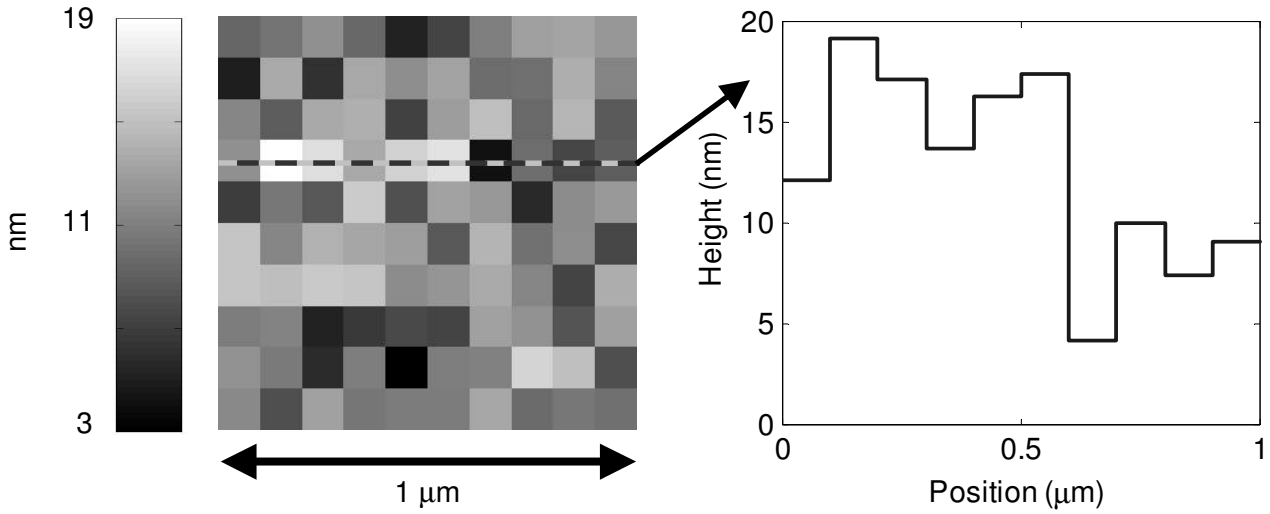

Fig 2. Exposure dataset definition for a deterministically fabricated Gaussian diffuser. The diffuser is defined as a grid of square cells where the height of each cell is assigned a random number from a Gaussian distribution limited to values falling within +/-3σ from the mean.

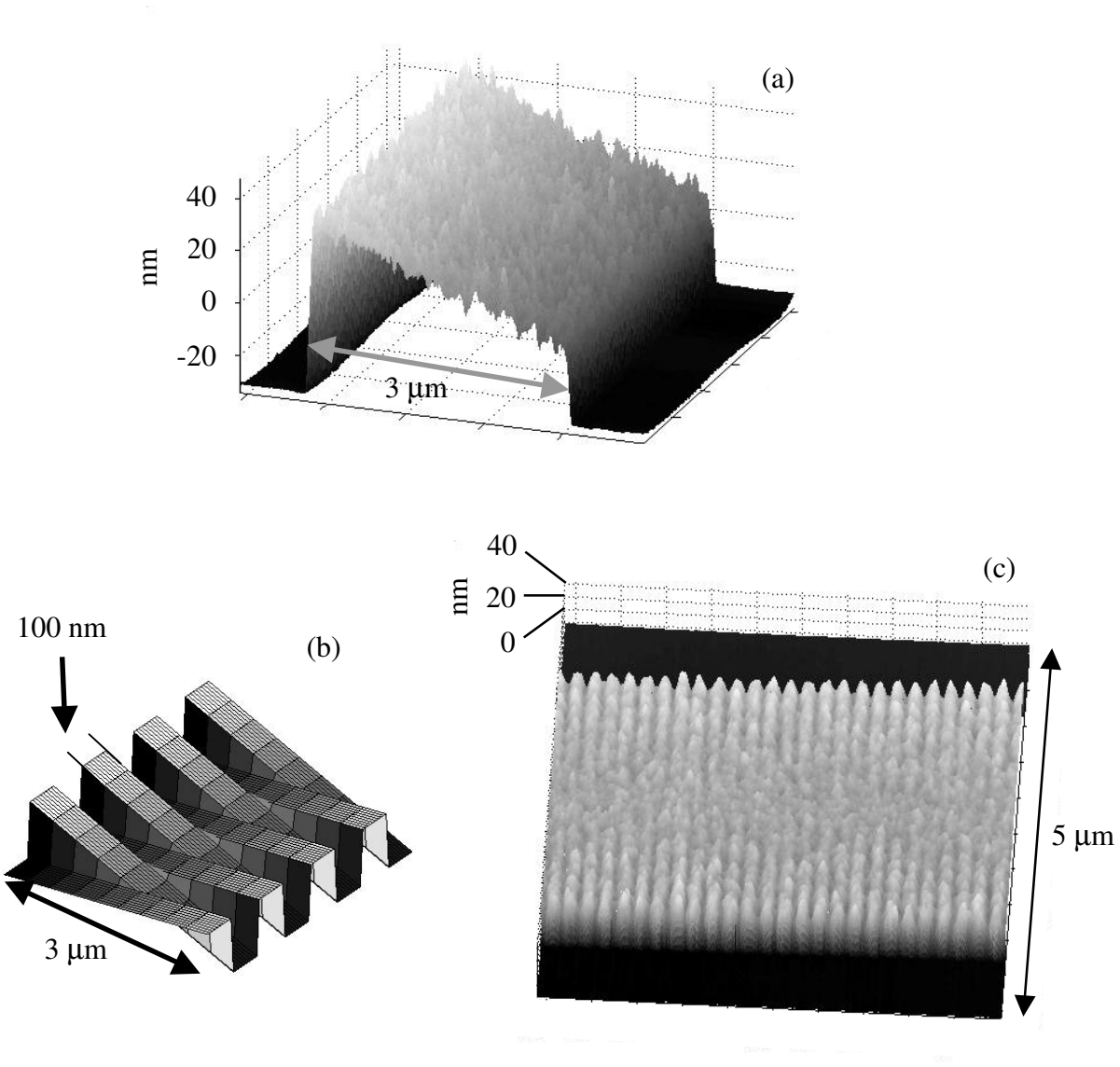

Fig 3. Demonstration of the relevance of proximity effects in small length scale direct gray-scale patterning of resist. (a) AFM image of patterned large 3-µm wedge in resist. Large features are relatively unaffected by proximity effects enabling the target 35-nm modulation to be achieved. (b) Prescription for alternating polarity 100-nm wide wedge pattern and (c) AFM image of corresponding patterned structure in resist suffering from approximately 10% loss in modulation.

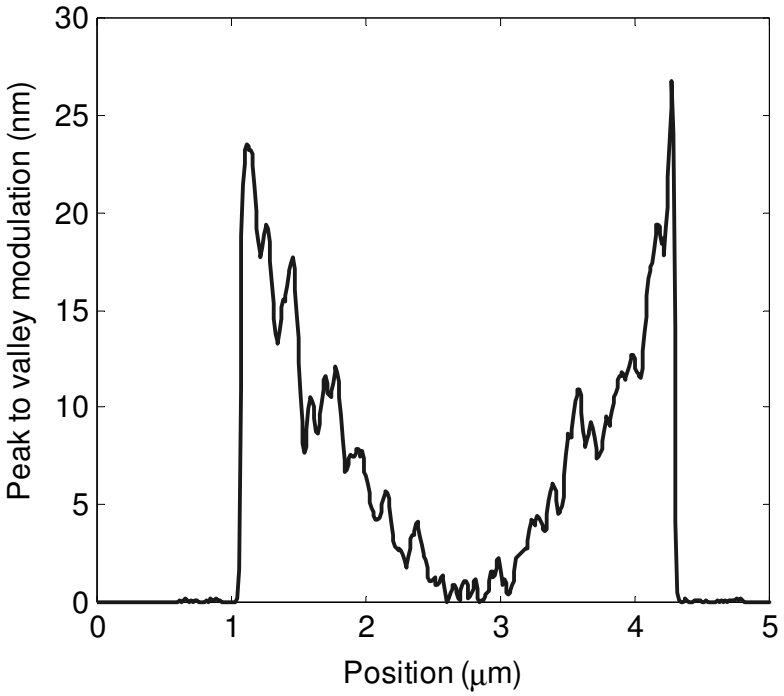

Fig 4. Calculated position dependent peak-to-valley modulation from the AFM image in Fig. 3(c). Each point in the plot corresponds to a separate row in the patterned structure from Fig. 3(c). The high modulation edges in the plot correspond the top and bottom rows the structure in Fig. 3(c) and the low modulation center of plot corresponds to central row in the patterned structure.

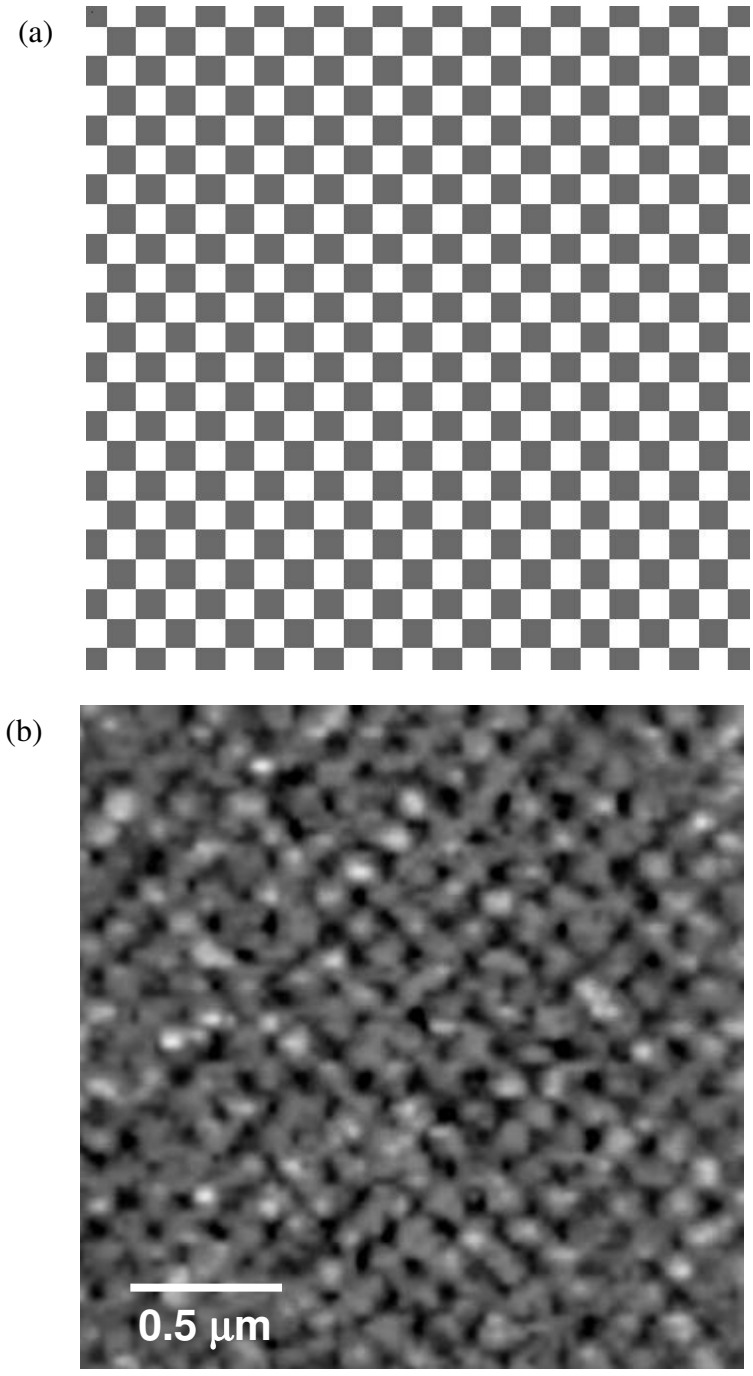

Fig 5. Representative exposure pattern (a) and AFM image of print (b) for modulation calibration accounting for proximity effects. The exposure pattern is a checkerboard comprised of 100-nm squares at two different doses. The complete calibration is based on a series of exposures each with a different relative dose between the two levels. The process is also repeated for a series of different nominal dose values.

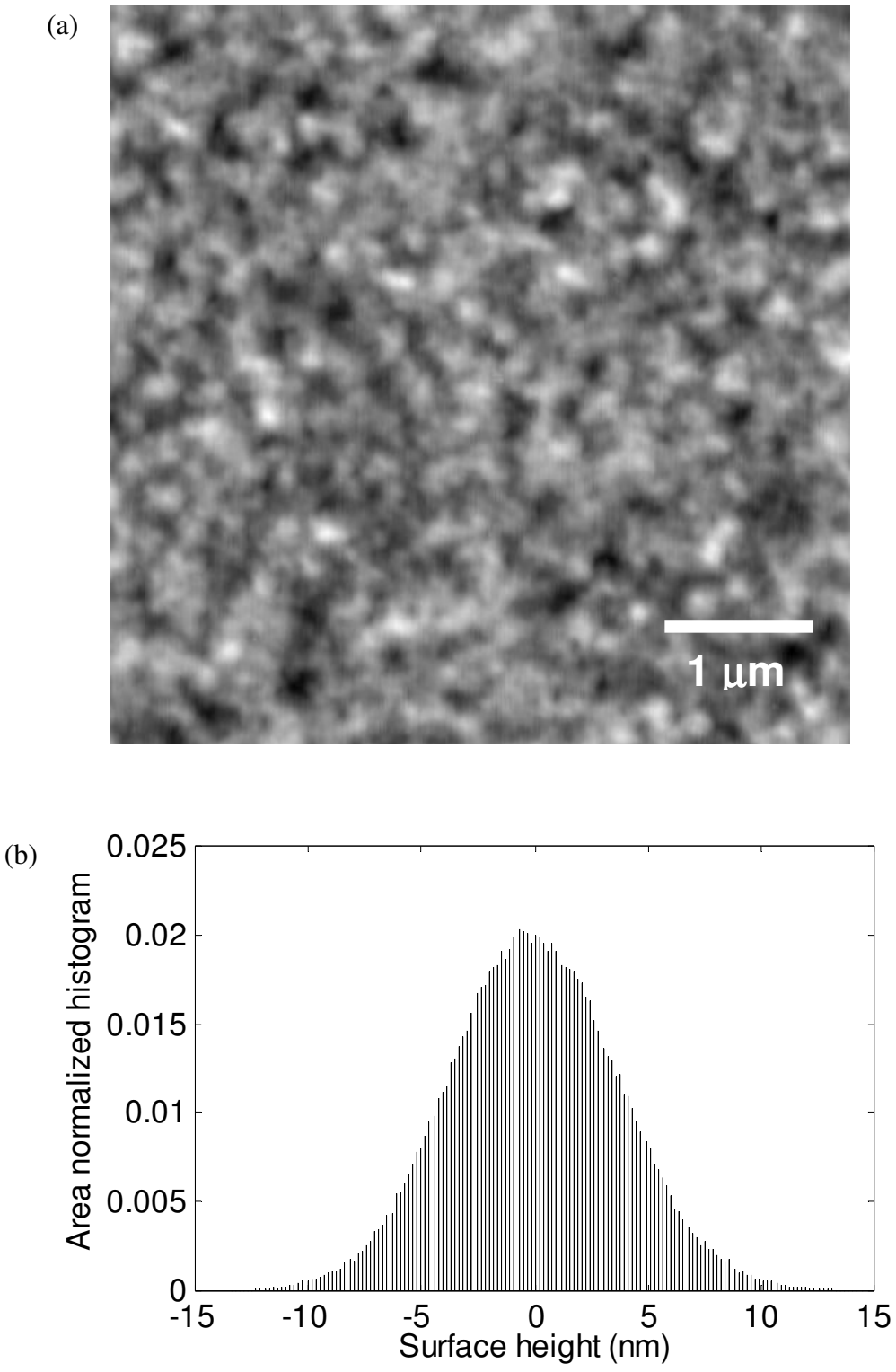

Fig 6. (a) AFM image of multiplayer coated HSQ diffuser and (b) normalized histogram of height distributions (approximation of the probability density function).

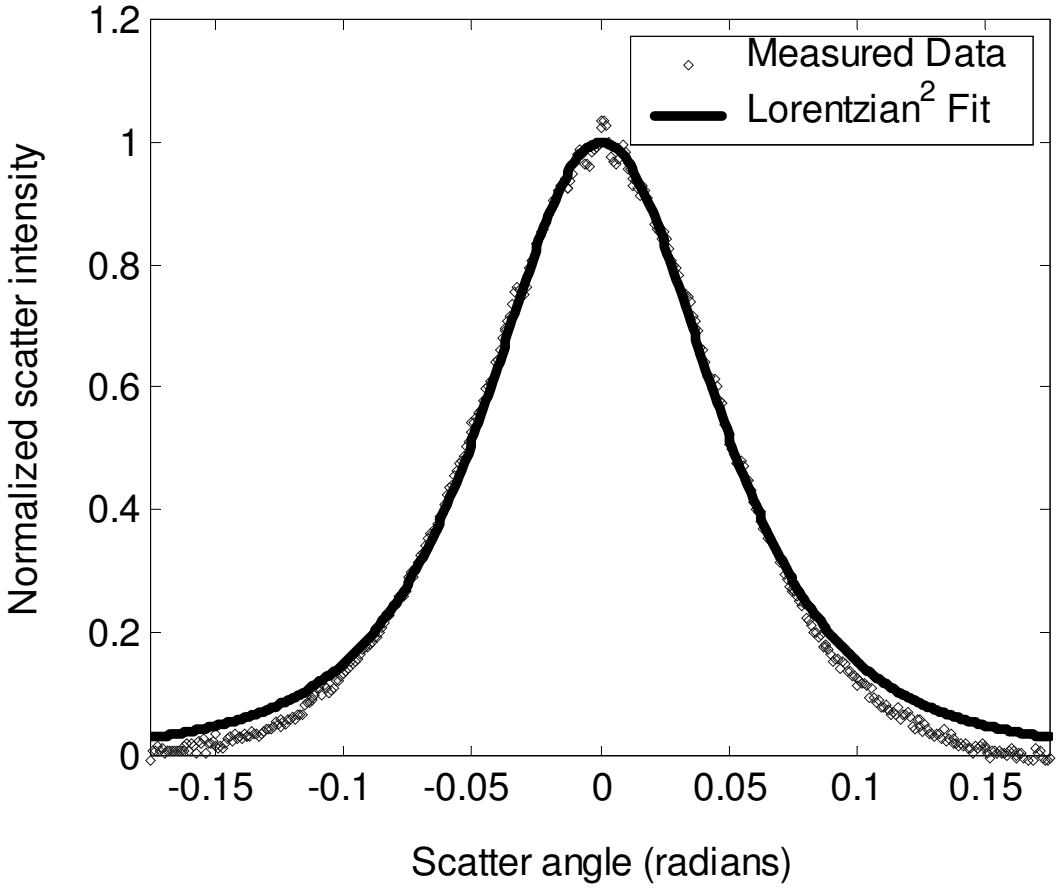

Fig 7. Line scan through the center of the measured far-field EUV diffraction pattern from the e-beam fabricated diffuser. No significant specular peak is observed. The measured total efficiency of the diffuser is 20.6% and the efficiency within the target 100-nm correlation length (0.059 radian collection angle) is 10.3%.

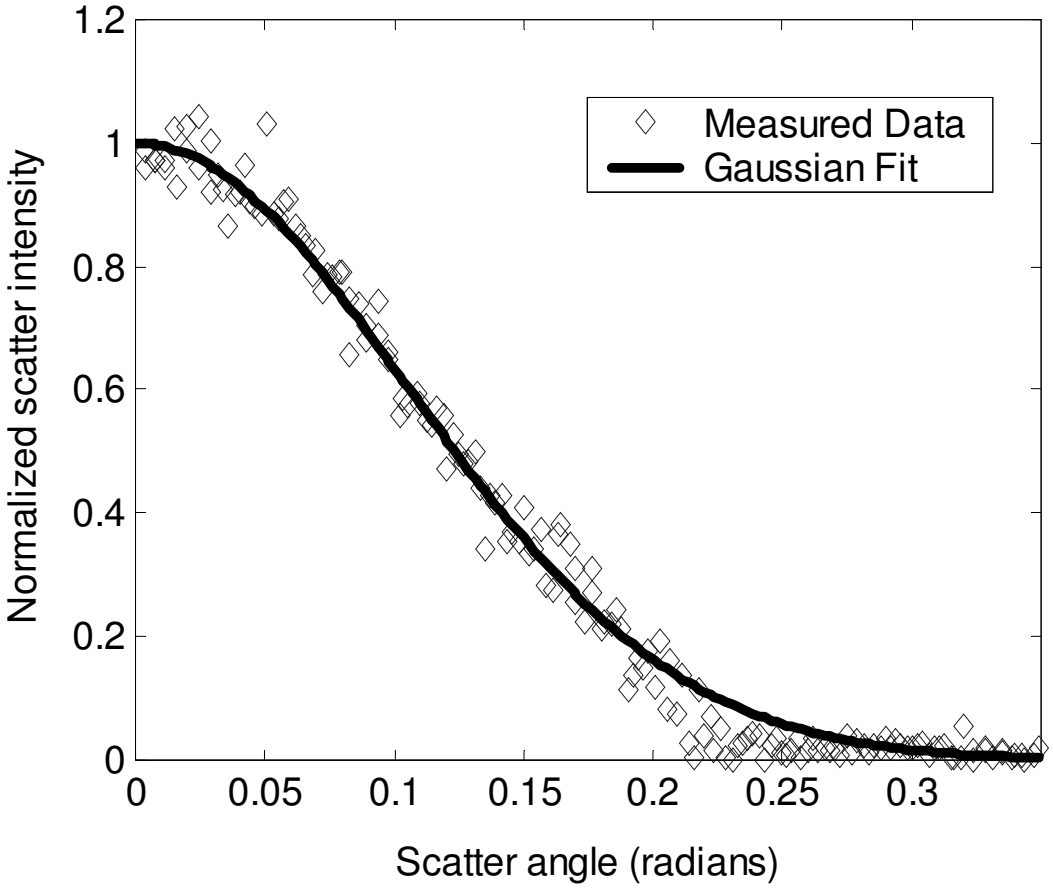

Fig 8. Line scan through the center of the measured far-field EUV diffraction pattern from the sputtered chrome diffuser. No significant specular peak is observed. The measured total efficiency of the diffuser is 14.9% and the efficiency within the target 100-nm correlation length (0.059 radian collection angle) is 2.2%.